General Disclaimer

One or more of the Following Statements may affect this Document

- This document has been reproduced from the best copy furnished by the organizational source. It is being released in the interest of making available as much information as possible.

- This document may contain data, which exceeds the sheet parameters. It was furnished in this condition by the organizational source and is the best copy available.

- This document may contain tone-on-tone or color graphs, charts and/or pictures, which have been reproduced in black and white.

- This document is paginated as submitted by the original source.

- Portions of this document are not fully legible due to the historical nature of some of the material. However, it is the best reproduction available from the original submission.

Produced by the NASA Center for Aerospace Information (CASI)

(NASA-TM-84982) POSTGLACIAL REBOUND OBSERVED BY LAGEOS AND THE EFFECTIVE VISCOSITY OF THE LOWER MANTLE (NASA) 39 p
HC A03/MF A01 CSCL 08G

N84-15705

Unclas
G3/46 42678

NASA

Technical Memorandum 84982

Postglacial Rebound Observed by Lageos and the Effective Viscosity of the Lower Mantle

David Parry Rubincam

FEBRUARY 1983

National Aeronautics and
Space Administration

Goddard Space Flight Center
Greenbelt, Maryland 20771

POSTGLACIAL REBOUND OBSERVED BY LAGEOS AND THE EFFECTIVE VISCOSITY OF THE LOWER MANTLE

David Parry Rubincam

Geodynamics Branch, Code 921
Goddard Space Flight Center
Greenbelt, MD 20771

ABSTRACT

Postglacial rebound appears to have been observed gravitationally by the Lageos satellite. Sixty-four observations of the orbital node made over a five year time interval reveal an acceleration of $(-8.1 \pm 1.8) \times 10^{-8}$ arcseconds day^{-2} due to a source which is not presently modeled in the GEODYN orbit determination computer program. This acceleration cannot be explained by the ocean tide with 18.6 year period, assuming it to be an equilibrium tide. Instead it seems to be due to postglacial rebound, which changes the J_2 coefficient in the spherical harmonic expansion of the earth's gravitational field at the rate of $(-8.2 \pm 1.8) \times 10^{-19}$ s^{-1}; this in turn accelerates the node. This rate does not agree with the -32×10^{-19} s^{-1} predicted by Wu and Peltier's (1982) L2 model, which has upper and lower mantle effective viscosities of 10^{21} and 10^{22} Pa s, respectively. It does agree well with their L1 model, which gives about -10×10^{-19} s^{-1}. Since the effective viscosity is 10^{21} Pa s throughout the entire mantle in the L1 model, the results support the contentions that (1) the effective viscosity is near 10^{21} Pa s everywhere in the mantle, and (2) this relatively low value for the effective viscosity may have permitted several degrees of polar wander due to glaciation during the Quaternary Ice Age.

PRECEDING PAGE BLANK NOT FILMED

POSTGLACIAL REBOUND OBSERVED BY LAGEOS AND THE EFFECTIVE VISCOSITY OF THE LOWER MANTLE

INTRODUCTION

During the Quaternary Ice Age the changing distribution of surface loads caused by the growth and decay of ice sheets deformed the earth. The deformation in turn altered the earth's gravitational field. The remnants of these effects provide information on the earth's rheology. In particular, ancient shorelines and the present-day free air gravity anomalies associated with the postglacial rebound of Laurentide Canada and Fennoscandia (see Plates 1 and 2) provide information on the earth's effective viscosity. Indeed, the relationship between deformation, gravity, and effective viscosity is a classical subject in geophysics (see, e.g., Cathles, 1975; Peltier, 1981; Peltier et al., 1978; Wu and Peltier, 1982; and references contained therein.) The value of the effective viscosity of the mantle has, of course, important implications for mantle convection and polar wander (e.g., Goldreich and Toomre, 1969; Peltier, 1980; and Lambeck, 1980). If the effective viscosity of the mantle is too high, then neither mantle convection nor polar wander will occur.

The purpose of the present investigation is to infer the effective viscosity of the mantle using satellite data. It involves looking at the rate of change of the earth's gravitational field as deduced from observations of the Lageos satellite. The basic idea here is that the postglacial rebound presently occurring changes the earth's gravitational field as well as its geometric shape. The changing gravitational field in turn affects the orbits of satellites. Since the rate of rebound is controlled in part by the effective viscosity of the mantle, observations of satellite orbits can in principle give information about the effective viscosity (e.g., Rubincam, 1979, pp. 6223-6224, and O'Keefe et al., 1979; see also Paddack, 1967 and Kozai, 1966.) In particular, postglacial rebound decreases J_2, the second degree, zeroth order term in the spherical harmonic expansion of the earth's

gravitational field; the earth is becoming less flattened. The decrease in J_2 should manifest itself as an acceleration $\ddot{\Omega}$ in the node Ω of a satellite's orbit as the node progresses along the equator.

Satellite laser ranging data obtained over a 5 year time interval reveals that in fact the node of Lageos' orbit is undergoing an acceleration due to a source which is not presently modeled in the orbit determination computer program. The acceleration is presumably due to postglacial rebound and the ocean tide with 18.6 year period; neither of these are contained in the program. A detailed analysis of the ocean tide with 18.6 year period, given in the Appendix, indicates that it contributes little to $\ddot{\Omega}$ over the time interval considered, assuming the tide to be an equilibrium one. After removing the tidal signal an acceleration still remains of $\ddot{\Omega} = (-8.1 \pm 1.8) \times 10^{-8}$ arcseconds day^{-2} which is assumed to be due to postglacial rebound; this means that the rate at which J_2 is changing with time is $\dot{J}_2 = dJ_2/dt = (-8.2 \pm 1.8) \times 10^{-19}$ s^{-1}. This value is about half that found by Yoder et. al. (1983), who also investigate $\dot{J}_2$ from Lageos observations.

The observed value for $\dot{J}_2$ is compared to the values predicted by the L1 and L2 earth models of Wu and Peltier (1982). Both of these realistic models are based on the Maxwell rheology and fit the Laurentide gravity anomaly and ancient shoreline data fairly well. The L1 model has an effective viscosity for the lower mantle of 10^{21} Pa s (10^{22} P), while the L2 model has a 10^{22} Pa s lower mantle. An upper limit on $\dot{J}_2$ for L1 and L2 is estimated from modeling the postglacial rebound of Laurentide Canada, which is where the major ice sheet of the Quaternary Ice Age rested. The Laurentide ice sheet is assumed to be a surface mass layer in the shape of a spherical cap whose mass waxes and wanes according to the ramp functions shown in Fig. 3. A lower limit on $\dot{J}_2$ for the L1 and L2 models is obtained from assuming that glaciation in other parts of the world, especially Antarctica, can reasonably be expected to give a total effect on $\dot{J}_2$ which is 3 times larger than that due to the Laurentide ice sheet alone. A (weakly) preferred value for $\dot{J}_2$ between the upper and lower limits is 5/3 that of the Laurentide ice sheet.

These considerations lead to the following results. For model L1, -17.9×10^{-19} s$^{-1} \leq \dot{J}_2 \leq -5.9 \times 10^{-19}$ s^{-1}, with a preferred value of -9.8×10^{-19} s^{-1}. These values agree quite well with the observed value of $(-8.2 \pm 1.8) \times 10^{-19}$ s^{-1}. For model L2, -58.4×10^{-19} s$^{-1} \leq \dot{J}_2 \leq -19.2 \times 10^{-19}$ s^{-1}, with a preferred value of -32.0×10^{-19} s^{-1}. This model makes J_2 decrease much too fast in comparison to the observed value. Hence of the two, the L1 model with its 10^{21} Pa s lower mantle effective viscosity is preferred to the L2 model with its 10^{22} Pa s lower mantle. This indicates that there is little difference in the effective viscosities of the upper and lower mantle, a result supported by the recent studies of Yuen et. al. (1982) and Peltier and Wu (1983). Also, a 10^{21} Pa s mantle allows a significant amount of polar wander due to glaciation – perhaps several degrees worth over the last few million years (Nakiboglu and Lambeck, 1980, 1981; Sabadini and Peltier, 1981; and Sabadini et al., 1982a, 1982b).

LAGEOS NODAL ACCELERATION

Lageos was launched into orbit on 4 May 1976 for the purpose of measuring crustal movements, plate motion, polar motion, and earth rotation (Smith and Dunn, 1980; Rubincam, 1982). The semimajor axis of Lageos' orbit is 1.227×10^7 m (about 2 earth radii) and its eccentricity is 0.004 (a nearly circular orbit). The orbital inclination with respect to the earth's equator is 109.9 degrees, while the rate at which the node of the orbit progresses along the equator is $\dot{\Omega} = +0.343$ degrees day^{-1}.

The data consist of 64 observations of nodal residuals spread over a 5 year time interval from 1976 to 1981 (Fig. 1). These values are what remain to be explained after running the laser range data through the GEODYN orbit determination computer program and after empirically determining and removing the K_1, K_2, P_1, and S_2 tides (solid earth plus ocean) from the remaining signal (Peter J. Dunn, private communication, 1982). These tides have periods (from the satellites's point of view) of 1051, 521, 221, and 280 days, respectively. The data points of Fig. 1 show a linear trend plus a slight curvature. Part of the slope can be explained by assuming that the value

for J_2 used in the GEODYN program needs a slight adjustment. The remaining part of the linear trend plus the curvature are presumably due to postglacial rebound and the 18.6 year period ocean tide, since neither of these are modeled in GEODYN. The 18.6 year tide is the only one which can contribute significantly to the curvature. It is accordingly investigated next, before proceeding to postglacial rebound.

This tide is due to the precession of the lunar orbit about the ecliptic. It is probably an equilibrium tide because of its long period (Proudman, 1960). Analysis of tidal records indicates that its amplitude is in fact close to its equilibrium value (Currie, 1976; Rossiter, 1967). Moreover, Agnew and Farrell (1978) find that the amplitude of the equilibrium tide on an earth with continents is about the same for an earth with a global ocean. Hence on the basis of these studies it appears that the most reasonable way to handle the data is to assume that the 18.6 year tide is an equilibrium one with an amplitude equal to that for the global ocean tide and subtract its effect from the data. In this case the perturbation in the node of Lageos' orbit is (see the Appendix)

$$\Delta\Omega^{O} = 0.224 \sin \hat{\Omega}^{*} \text{ arcseconds} \qquad (1)$$

where $\hat{\Omega}^{*}$ is the node of the moon's orbit measured with respect to the ecliptic and the superscript "O" stands for "Ocean." A plot of (1) (Fig. 1, solid curve) shows that $\Delta\Omega^{O}$ varies almost linearly with time over the time interval of the data points. This is due to the fact that during this time $\Delta\Omega^{O}$ is rising from a trough to a peak and to the long period of the tide. Hence the ocean tide contributes mostly to the slope of the data points and only a little to the curvature.

The signal remaining after the ocean tide contribution (1) is subtracted out is presumably due to postglacial rebound and the slight error in the value of J_2. Thus its functional form should be

$$\Delta\Omega = \Omega_0 + \dot{\Omega}_0 T + (1/2)\, \ddot{\Omega}\, T^2$$

where T is the elapsed time since MJD (Modified Julian Date) 42904, Ω_0 is a constant, $\dot{\Omega}_0$ is the slope, and $\ddot{\Omega}$ is the desired acceleration of the node due to postglacial rebound. A standard least squares fit to the modified data yields $\Omega_0 = 0.10 \pm 0.02$ arcseconds, $\dot{\Omega}_0 = (5.7 \pm 0.2) \times 10^{-4}$ arcseconds day^{-1}, and

$$\ddot{\Omega} = (-8.1 \pm 1.8) \times 10^{-8} \text{ arcseconds day}^{-2}$$

$$= (-5.3 \pm 1.2) \times 10^{-23} \text{ rad s}^{-2} \qquad (2)$$

Fig. 2 shows the curvature in the data with the constant, slope, and ocean tide removed.

It remains to find $\dot{J}_2$ from (2). This is easily done, since the rate $\dot{\Omega}$ at which the node of a near-earth satellite's orbit progresses along the equator is proportional to J_2 (e.g., Kaula, 1968, p. 174). Hence it follows by differentiation that $\dot{J}_2/J_2 = \ddot{\Omega}/\dot{\Omega}$, so that

$$\dot{J}_2 = (-8.2 \pm 1.8) \times 10^{-19} \text{ s}^{-1} \qquad (3)$$

after using (2) and the numerical values $J_2 = 1.0826 \times 10^{-3}$ (Stacey, 1977, p. 332) and $\dot{\Omega} = +0.343$ degrees day^{-1}. This is the value for $\dot{J}_2$ which is assumed to be due to postglacial rebound.

EARTH MODELS

What must be done now is to estimate $\dot{J}_2$ for Wu and Peltier's (1982) earth models L1 and L2 to see whether they agree with the observed value given by (3). This will be done by first considering the effect of postglacial rebound in Laurentide Canada on the gravitational field. This will provide an upper bound on $\dot{J}_2$ (remembering that it is a negative number), since Laurentide Canada is only a partial (though probably the major) contributor to $\dot{J}_2$. Past glaciations in other regions of the earth, such as Fennoscandia, Siberia, and Antarctica also contribute to $\dot{J}_2$. Considerations of these other regions, based mostly on the maximum drop in global sea level, then lead to a lower

limit on $\dot{J}_2$. Finally, a (weakly) preferred value for $\dot{J}_2$ between the upper and lower limits for each of the models will be found.

The Laurentide gravity anomaly near Hudson Bay is quite apparent on the GEM 10B free air gravity anomaly map (Plates 1 and 2). The GEM 10B field is based on satellite ranging, satellite altimetry, and surface gravity data (Lerch et al., 1981); "GEM" stands for "Goddard Earth Model." The gravity anomalies were computed from the standard equation (e.g., Rapp, 1975, p. 198)

$$\Delta g = \gamma \sum_{\ell=2}^{\infty} (\ell-1) \sum_{m=0}^{\ell} (\bar{C}_{\ell m} \cos m\lambda + \bar{S}_{\ell m} \sin m\lambda) \bar{P}_{\ell m} (\cos \theta)$$

(written here in normalized form) using the GEM 10B gravitational field coefficients ($\bar{C}_{\ell m}$, $\bar{S}_{\ell m}$) given by Lerch et al. (1981) up to and including degree and order 36, except for the $\ell = 2, 4$, $m = 0$ terms. For these terms the hydrostatic values $\bar{C}_{20}^{H} = -480.516 \times 10^{-6}$ and $\bar{C}_{40}^{H} = +1.212 \times 10^{-6}$ derived from Nakiboglu (1979, p. 645) were subtracted from the corresponding GEM 10B values. Hence the anomalies shown in Plates 1 and 2 are basically referred to the earth's hydrostatic figure. The underlying maps shown in the plates are the tectonic activity maps of Lowman (1981, 1982).

Note that the gravity low in Laurentide Canada reaches a minimum value of about -50×10^{-5} m s^{-2} (−50 mgal) when referred to the hydrostatic flattening. This is in contrast to the usual -40×10^{-5} m s^{-2} when referred to the reference flattening f = 1/298.255 (e.g., Wu and Peltier, 1982; Peltier and Wu, 1982; Rapp, 1975, p. 210).

The ancient Laurentide ice sheet is modeled here as a surface mass layer σ^{ICE} of constant density and in the shape of a spherical cap. The angular radius of the cap is α and its center is located at colatitude β. The mass M of the ice sheet varies with time t according to the equation $M = M_0 f(t)$, where M_0 is a constant and equal to the maximum mass of the ice sheet and f(t) is shown in Fig. 3. The function f(t) represents a simplified version of the glaciation-deglaciation

history of Laurentide Canada (Sabadini and Peltier, 1981). The ramp functions of Fig. 3 are characterized by the constants T_1 and T_2. The accretion time T_1 is ~100 000 years and the disintegration time T_2 is ~10 000 years. The time $T_3 \cong 5000$ years is the elapsed time since the disappearance of the last ice sheet. Also, the cycles extend about 2 million years into the past (e.g., Wu and Peltier, 1982, p. 480.)

The water composing the ice sheet comes from the oceans, assuming a closed hydrologic cycle Hence the oceans must also be represented as a surface mass layer σ^{OC} which varies with time. Sabadini and Peltier (1981, p. 558) give the equations for σ^{ICE} and σ^{OC}. Adding them together to obtain the total mass layer $\sigma = \sigma^{ICE} + \sigma^{OC}$ yields

$$\sigma = \sum_{\ell=1}^{\infty} \sigma_\ell(\theta', t)$$

where

$$\sigma_\ell(\theta', t) = \frac{M_0 f(t)}{2\pi R_E^2} \left[\frac{(2\ell+1)}{\ell(\ell+1)} \frac{\partial P_{\ell 0}(\cos\alpha)}{\partial(\cos\alpha)}\right] P_{\ell 0}(\cos\theta'). \tag{4}$$

Here $P_{\ell 0}(\cos\theta')$ is the associated Legendre polynomial of degree ℓ and order 0, θ' is the angle measured from the center of the cap, and R_E is the radius of the earth.

The effect of this ice sheet on the present-day exterior gravitational field must now be found. It will be given by

$$V_\ell' = \left(\frac{R_E}{r}\right)^3 \int_{-\infty}^{t} \sigma_\ell(\theta'', t') \, G_\ell(\psi, t-t') \, dA'' \, dt' \tag{5}$$

where V_ℓ' is the term of degree ℓ in the spherical harmonic expansion of the gravitational potential about the axis of the cap, r is the radial distance, dA'' is the element of area, and $G_\ell(\psi, t-t')$ is the Green function (Wu and Peltier, 1982, pp. 468-469)

$$G_\ell(\psi, t-t') = G_\ell^E(\psi, t-t') + G_\ell^V(\psi, t-t')$$

where

$$G_\ell^E(\psi,t-t') = \frac{G}{R_E}\, k_\ell^E\, \delta(t-t')\, P_{\ell 0}(\cos\psi) \tag{6}$$

and

$$G_\ell^V(\psi,t-t') = \frac{G}{R_E} \sum_{j=1}^{K} r_j^\ell\, e^{-s_j^\ell (t-t')}\, P_{\ell 0}(\cos\psi) \tag{7}$$

Here G is the universal constant of gravitation, G_ℓ^E is the elastic part of the Green function, k_ℓ^E is the elastic Love number, $\delta(t-t')$ is the Dirac delta function, G_ℓ^V is the viscous part of the Green function, ψ is the angle from the load point to the point of observation, K is the number of relaxation modes, and the r_j^ℓ and s_j^ℓ are numbers which characterize the particular earth model and are discussed below. The associated Legendre polynomial $P_{\ell 0}(\cos\psi)$ can be written

$$P_{\ell 0}(\cos\psi) = \sum_{m=0}^{\ell} \frac{(2-\delta_{0m})\,(\ell-m)!}{(\ell+m)!}\, P_{\ell m}(\cos\theta'')\, P_{\ell m}(\cos\theta') \cdot [\cos m\lambda'' \cos m\lambda' + \sin m\lambda'' \sin m\lambda'] \tag{8}$$

using the addition theorem for spherical harmonics (e.g., Kaula, 1968, p. 67). Here θ'' and θ' are colatitudes and λ'' and λ' are east longitudes measured with respect to the axis of the cap.

The elastic part (5) of the Green function is of no interest here and will not be considered further. Also, it proves to be slightly more convenient to use $\kappa_j^\ell = 1/r_j^\ell$ and $\tau_j^\ell = 1/s_j^\ell$ rather than r_j^ℓ and s_j^ℓ; the numbers which characterize the earth are now measured in years rather than inverse years. Further, only the $\ell = 2$ parts of (4), (5), (7), and (8) need be found since this investigation is concerned only with the second degree term in the potential. Hence setting $\ell = 2$ in these equations, using (8) in (7), (4) and (7) in (5), and carrying out the integration over area gives

$$V_2' = \frac{GM_o}{R_E}\left(\frac{R_E}{r}\right)^3 \cos\alpha \left\{ \sum_{j=1}^{K} \frac{e^{-t/\tau_j^2}}{\kappa_j^2} \left[\int_{-\infty}^{t} f(t')\, e^{-t'/\tau_j^2}\, dt' \right] \right\} P_{\ell 0}(\cos\theta')$$

where $\partial P_{20}(\cos\alpha)/\partial(\cos\alpha) = 3\cos\alpha$ has been used.

ORIGINAL PAGE IS
OF POOR QUALITY

Applying the addition theorem (8) once again to express the potential in terms of spherical harmonics about the rotation axis of the earth rather than the axis of the cap and evaluating the time integral using the function shown in Fig. 3 yields

$$V_2^L = \frac{GM_E}{R_E} J_2^L \left(\frac{R_E}{r}\right)^3 P_{20}(\cos\theta)$$

where

$$J_2^L = \frac{M_o}{M_E} \cos\alpha \left(\frac{3}{2}\cos^2\beta - \frac{1}{2}\right)$$

$$\cdot \left\{ \sum_{j=1}^{K} \left[\frac{(\tau_j^2)^2}{\kappa_j^2} \right] \left[\frac{1}{T_2} + \frac{e^{-N(T_1+T_2)/\tau_j^2}}{T_1} + \left(\frac{1}{T_1}+\frac{1}{T_2}\right) \left(\frac{1-e^{-T_1/\tau_j^2} + e^{[-N(T_1+T_2)+T_1]/\tau_j^2} - e^{-(N-1)(T_1+T_2)/\tau_j^2}}{e^{(T_1+T_2)/\tau_j^2} - 1} \right) \right] \right.$$

$$\left. \cdot \left[e^{-T_3/\tau_j^2} \right] \right\} \qquad (9)$$

Here V_2^L is the desired second degree coefficient in the potential, θ is colatitude measured from the North Pole, M_E is the mass of the earth, N is the number of glacial cycles, and the superscript "L" on V_2^L and J_2^L stands for "Laurentide." Use has been made of the expression $S = (1 - X^N)/(1 - X)$, where $S = 1 + X + X^2 + \ldots + X^{N-1}$, in evaluating the time integral. Taking the derivative of (9) with respect to time T_3 finally gives

$$\dot{J}_2^L = -\frac{M_o}{M_E} \cos\alpha \left(\frac{3}{2}\cos^2\beta - \frac{1}{2}\right)$$

$$\cdot \left\{ \sum_{j=1}^{K} \left[\frac{\tau_j^2}{\kappa_j^2} \right] \left[\frac{1}{T_2} + \frac{e^{-N(T_1+T_2)/\tau_j^2}}{T_1} + \left(\frac{1}{T_1}+\frac{1}{T_2}\right) \left(\frac{1-e^{-T_1/\tau_j^2} + e^{[-N(T_1+T_2)+T_1]/\tau_j^2} - e^{-(N-1)(T_1+T_2)/\tau_j^2}}{e^{(T_1+T_2)/\tau_j^2} - 1} \right) \right] \right.$$

$$\left. \left[e^{-T_3/\tau_j^2} \right] \right\} \qquad (10)$$

as the rate of change of J_2 due only to the Laurentide ice sheet.

The question now arises as to what values to use for the parameters appearing in (10). The values for M_0, β, and α are taken from Sabadini et al. (1982a, p. 2897) and are given in Table 1. The values for T_1, T_2, and T_3, also given in Table 1, are estimated from Fig. 2 of Andrews and Berry (1978), which shows the last glaciation-deglaciation cycle of the Quaternary Ice Age. The times T_1 = 112 000 and T_2 = 13 000 years are somewhat longer than those used by Sabadini and Peltier (1981), whose values of 90 000 and 10 000 years are more in accord with the period of the eccentricity cycle of the earth's orbit which apparently drives the glaciation (Hays et al. 1976). The longer times are used here since the last accretion-disintegration cycle is the most important; the earth will not "remember" much of the previous cycles for the relatively low effective viscosities considered here (Sabadini and Peltier, 1981, p. 568). The implications of using the shorter astronomical times will be discussed below. The Ice Age extends about 2 million years into the past, so $N \cong 20$ (e.g., Wu and Peltier, 1982, p. 480). The values for M_E and R_E come from Stacey (1977, pp. 331-332).

The values for $\tau_j^2 = 1/\nu_j^2$ and $\tau_j^2/\kappa_j^2 = r_j^2/s_j^2$ for the L1 and L2 models are derived from Wu and Peltier (1982, pp. 465-466) and are shown in Table 2. Both models have the same density and elastic properties as model 1066B of Gilbert and Dziewonski (1975). Model L1 has a 120 km thick lithosphere, a mantle with effective viscosity of 10^{21} Pa s, and an inviscid core. Model L2 is the same as L1 except that the effective viscosity of the mantle below the density discontinuity at 671 km depth is 10^{22} Pa s. The multiple relaxation modes are due to the discontinuities present in the models: M0 is the fundamental mantle mode, M1 and M2 are due to the density discontinuities at 671 km and 420 km depth, respectively, and L0 and C0 are due to the presence of the lithosphere and the core, respectively. Both the L1 and L2 models fit the Laurentide gravity anomaly referred to the nonhydrostatic figure and bracket the relative sea level data, leading Wu and Peltier (1982) and Peltier and Wu (1982) to conclude that the effective viscosity of the lower mantle is between 10^{21} and 10^{22} Pa s.

Using the numerical values given in Tables 1 and 2 in (10) yield the following results. For model L1

$$\dot{J}_2^L = -5.9 \times 10^{-19}\ s^{-1} \tag{11}$$

while for model L2

$$\dot{J}_2^L = -19.2 \times 10^{-19}\ s^{-1} \tag{12}$$

for postglacial rebound due to Laurentide Canada alone. Note that model L2 already predicts a rate of decrease in J_2 which is over twice the observed value given in (3), while model L1 predicts a rate which is slightly less than the observed value.

The rates given by (11) and (12) must be considered upper bounds on $\dot{J}_2$, since Laurentide Canada is not the only region to have had an ice sheet. Other parts of the globe underwent glaciation as well and will also contribute to $\dot{J}_2$. A rough estimate of their contributions will be considered next.

The maximum drop in global sea level was probably about 80 m and may have been as high as 120 m (e.g., Andrews and Berry, 1978, p. 210). It can easily be shown that the Laurentide ice sheet accounts for only 48 m or so of this drop, assuming that the ice sheet had the mass given in Table 1; other ice sheets must account for the remaining 32 to 72 m. Certainly a lower limit on $\dot{J}_2$ can be obtained by assuming that 72 m was due to an ice sheet comparable to the Laurentide ice sheet situated in Antarctica over the South Pole. (There are in fact large Antarctic anomalies which may be at least partially explained by glaciation; see Plate 2). This maximizes the effect on $\dot{J}_2$ not only by maximizing the allowable mass but also by placing it at the pole (the angle β in (10) is now 180 degrees rather than 25 degrees). Use of (10) gives this hypothetical ice sheet an effect on $\dot{J}_2$ which is about twice that of the Laurentide ice sheet; thus the total effect on $\dot{J}_2$ is about $3\dot{J}_2^L$ so that

$$-17.9 \times 10^{-19}\ s^{-1} \leqslant \dot{J}_2 \tag{13}$$

for model L1 and

$$-58.4 \times 10^{-19}\ s^{-1} \leqslant \dot{J}_2 \tag{14}$$

for model L2. These calculations are rough since they assume an Antarctic ice sheet with the same radius as the Laurentide ice sheet (but with 1.5 times the mass) and the same history; they also assume that the effect of each ice sheet may be calculated independently of the other, i.e. there is no coupling between the two. However, only rough estimates are desired because the uncertainties of the sea level data make further refinements not worthwhile.

Preferred values for $\dot{J}_2$ for models L1 and L2 will now be found. The Fennoscandian, Siberian, and other ice sheets (excluding Antarctica) had a combined mass which was about 42 per cent that of the Laurentide ice sheet (O'Connell, 1971, p. 308) and accounted for about 20 m of the global drop in sea level. Hence by adding in the 48 m or so due to the Laurentide ice sheet about 48 + 20 = 68 m of the probable 80 m drop in global sea level can be explained. Thus by assuming that these other ice sheets in fact account for 32 m of an assumed 80 m total drop and by lumping them together into one ice sheet with the same radius and colatitude as the Laurentide ice sheet but with 2/3 the mass yields $\dot{J}_2 = (5/3)\,\dot{J}_2^L$. So for model L1

$$\dot{J}_2 = -9.8 \times 10^{-19}\ s^{-1} \tag{15}$$

and for model L2

$$\dot{J}_2 = -32.0 \times 10^{-19}\ s^{-1}. \tag{16}$$

These values are only weakly preferred due to the limitations of the calculations as discussed above and because a possibly substantial amount of deglaciation in Antarctica has been ignored (Sabadini et al., 1982a, pp. 2897-2898). Even so, the value (15) agrees well with the observed value (3), while (16) is a factor of 4 too large. Hence of the two models, L1 is preferred to L2.

DISCUSSION

It has been assumed here that the curvature evident in the nodal residuals is due mainly to postglacial rebound. There may of course be alternative ways of explaining the data. One such alternative which immediately comes to mind is the 18.6 year ocean tide; perhaps it is not an equilibrium tide as assumed here. In fact, Sanchez (1979) speculated that this tide may have an amplitude several times that of its equilibrium value in order to explain a polar motion component with the same period found by Markowitz (1979) from polar motion data.

The data shown in Fig. 1 were accordingly reanalyzed to investigate this possibility by assuming that the functional form of the nodal residuals is now given by

$$\Delta\Omega = \Omega_o + \dot{\Omega}_o T + \frac{1}{2}\ddot{\Omega}T^2 + A_1 \sin \hat{\Omega}^*.$$

Here the last term represents an 18.6 year ocean tide which is unconstrained in amplitude but constrained to having the equilibrium phase. In this case solving for Ω_o, $\dot{\Omega}_o$, $\ddot{\Omega}$, and A_1 gives $A_1 = 0.42 \pm 0.15$ arcseconds and $\ddot{\Omega} = (-5.9 \pm 2.5) \times 10^{-8}$ arcseconds day^{-2}, which would indicate that the tide has about twice its equilibrium amplitude given by (1). But this still does not explain the quadratic behavior of the residuals; the new value for $\ddot{\Omega}$ is not significantly changed from (2) and still agrees fairly well with Wu and Peltier's (1982) L1 model. Of course the ocean tide could be unconstrained in both amplitude and phase by adding a term of the form $A_2 \cos \hat{\Omega}^*$ to the above equation and solving for all of the coefficients, including A_2. In this case $\ddot{\Omega} = (4 \pm 100) \times 10^{-8}$ arcseconds day^{-2}, $A_1 = 0.44 \pm 0.23$ arcseconds and $A_2 = -0.12 \pm 1.3$ arcseconds, so that $\ddot{\Omega}$ is not significantly different from zero and no relaxation of the earth has been observed. However, it is unreasonable to solve for the amplitude and phase of a tide with an 18.6 year period with only 5 years worth of data. In any case the ocean tide would have to depart drastically from its equilibrium value in order to explain the Lageos observations.

A different ocean tide might appear to be another way of accounting for the T^2 behavior of the points in Fig. 1; but (A3) indicates that there is no tide of suitable period and amplitude to do so.

The deceleration of the earth's spin by tidal friction does not account for it either, as may be seen from the following considerations. For a homogeneous, liquid earth the hydrostatic flattening factor f^H is proportional to ω^2 to a first approximation, where ω is the angular speed of the earth (e.g., Lyttleton, 1953, p. 38). Further, elementary considerations show that also to a first approximation J_2 is proportional to f^H (e.g., Kaula, 1968, pp. 68-69). Hence by differentiation $\dot{J}_2/J_2 = 2\dot{\omega}/\omega$, where $\dot{\omega}$ is the acceleration of the rotation speed due to tidal friction. Using the values $\dot{\omega} \cong -6 \times 10^{-22}$ rad s^{-2} (Stacey, 1977, p. 99) and $\omega = 7.29 \times 10^{-5}$ rad s^{-1} (Stacey, 1977, p. 332) in this equation give $\dot{J}_2 \cong -2 \times 10^{-20}$ s^{-1}, which is a factor of 40 smaller than the observed rate given by (3). Thus even if the earth were completely fluid, the observed relaxation of the earth could not be due to the slowdown of its rotation rate by tidal friction.

There may be some other alternative, as yet unthought of, which will explain the data; but thus far postglacial rebound does quite well. Moreover, postglacial rebound predicts the continued quadratic behavior of the residuals in the future; its parabolic nature should become more and more evident as data is taken in future years. Hence the relaxation of the earth is an hypothesis which is easily tested.

The data show good agreement with Wu and Peltier's (1982) L1 model for the parameter values adopted here. It has been mentioned that the values of the accretion time T_1 = 112 000 years and disintegration time T_2 = 13 000 years are longer than the 90 000 years and 10 000 years used by Sabadini et al. (1982a, 1982b) and Sabadini and Peltier (1981). Use of these shorter times give a preferred $\dot{J}_2 = -12.5 \times 10^{-19}$ s^{-1} for the L1 model and -36.7×10^{-19} s^{-1} for the L2 model, as compared to the observed $(-8.2 \pm 1.8) \times 10^{-19}$ s^{-1}. Thus the shorter times, which appear to be

more in accord with the deep-sea sediment core data (e.g., Hays et al., 1976; Sabadini and Peltier, 1981, p. 566), worsen the agreement slightly, but not seriously, between the L1 and observed values.

The results given here can be compared to other recent studies. Yoder et al. (1983) have independently analyzed observations of Lageos' node and have concluded that $\dot{J}_2$ is about $(-16 \pm 3) \times 10^{-19}$ s^{-1}. This figure is twice as large as that found here, and falls between the preferred values (15) and (16) for the L1 and L2 models, arguing for a lower mantle effective viscosity between 10^{21} Pa s and 10^{22} Pa s. Also, Yuen et al. (1982) inferred the effective viscosity of the lower mantle from the observed nontidal acceleration of the earth's rotation. They find the effective viscosity to be between 1 and 4×10^{21} Pa s, in good agreement with the results given here. Finally, Peltier and Wu (1983) also calculate from rotational acceleration that it should be between 1.6 and 6×10^{21} Pa s. On the whole it appears that the effective viscosity of the lower mantle is indeed between 10^{21} Pa s and 10^{22} Pa s, with the present investigation supporting the lower value.

It is interesting to note that the L2 model has J_2 decay more rapidly than the L1 model, even though its effective mantle viscosity is a factor of 10 higher than that of the L1 model. This seemingly paradoxical behavior is due to the discontinuities present in these realistic models (Wu and Peltier, 1982, p. 475-476). This behavior also shows that previous attempts by Rubincam (1979) and O'Keefe et al. (1979) to derive the effective viscosity of the lower mantle from satellite data using an incompressible, homogeneous, viscous earth in the manner of Darwin (1879) are too simplistic. It can be shown that the classical Darwinian model applied to the Lageos data give an effective viscosity of about 10^{23} Pa s – far from the more reasonable value of 10^{21} Pa s. Hence the data cannot be inverted to give a unique effective viscosity. Instead realistic models must be constructed and then tested against observation.

It is also of some interest to compare the glacial flattening to the total nonhydrostatic flattening of the earth. Wu and Peltier (1982) do not give quite enough information in their Table 8 to compute J_2^L for the L1 model, but do in their Table 9 for the L2 model, which gives $J_2^L = 1.1 \times 10^{-6}$ by (10). (Both the L1 and L2 models agree with the gravity anomaly data referred the reference flattening and should give about the same value.) The preferred value is $J_2^L = 1.8 \times 10^{-6}$ with a maximum possible value of 3.3×10^{-6}. The total nonhydrostatic value ΔJ_2 for the earth is about 8.174×10^{-6}, as may be derived from Table 3 of Nakiboglu (1979). So the squashing of the earth by the glaciers of the Quarternary Ice Age accounts for between 13 per cent and 40 per cent of the present-day nonhydrostatic part of J_2, with a preferred value of 22 per cent. Wang (1966) had suggested that glaciation might account for all of ΔJ_2, but McKenzie (1966), Kaula (1967), and O'Connell (1971) indicated that glaciation accounts for an amount closer to the percentages given here. (For further discussion of ΔJ_2, see Goldreich and Toomre, 1969).

The support for the L1 model indicates that there is little, if any, jump in the effective viscosity across the density discontinuity at 671 km depth (Wu and Peltier, 1982; Peltier and Wu, 1982). Also, an effective viscosity of 10^{21} Pa s for the whole mantle has important implications for polar wander. Sabadini et al. (1982a, 1982b), Sabadini and Peltier (1981), and Nakiboglu and Lambeck (1980, 1981) find that glaciation on an earth with this value for the effective viscosity of the mantle could have caused several degrees of polar wander over the last few million years, and can explain the current movement of the pole towards Canada. This supposes, of course, that the linear Maxwell rheology assumed here applies to tectonic stresses and time scales, which may not be the case (e.g., Weertman, 1978; but see Wu and Peltier, 1982, p. 476). McAdoo (1982), for instance, finds that non-Newtonian flow best explains the geoid over subducting slabs.

SUMMARY

The node of Lageos' orbit is undergoing an acceleration not presently modeled in the orbit determination computer program. It appears to be caused by the postglacial rebound of the earth. An effective viscosity of 10^{21} Pa s for the whole mantle is consistent with the observed acceleration. This value for the effective viscosity allows rapid polar wander due to glaciation.

ACKNOWLEDGMENTS

I wish to thank David E. Smith for many helpful discussions on all aspects of this work. Peter J. Dunn generously supplied the Lageos data as well as information about GEODYN. I have also profited from discussions with Demos Christodoulidis, Dave McAdoo, and John A. O'Keefe. Barbara Putney aided with the computer programming.

APPENDIX

The problem addressed here is to find the effect of the 18.6 year global equilibrium ocean tide on the node Ω of Lageos' orbit as given by (1).

The amplitude of the global equilibrium ocean tide is (Agnew and Farrell, 1978, equation 2.5)

$$\zeta_2 = \frac{1 + k_2 - h_2}{1 - \frac{3\rho_W}{5\bar{\rho}_E}(1+k_2'-h_2')} \frac{U_2}{g}$$

where U_2 is the tide-raising potential at the earth's surface, $\rho_W = 1022$ kg m^{-3} is the density of sea water, and k_2, h_2, k_2', h_2' are the usual Love numbers. The ocean tide will produce a disturbing potential (Hendershott, 1972, equation 5)

$$(1+k_2')\, g\alpha_2\, \zeta_2 \left(\frac{R_E}{r}\right)^3$$

while the solid earth tidal disturbing potential is

$$k_2\, U_2 \left(\frac{R_E}{r}\right)^3$$

where $\alpha_2 = 3\rho_W / 5\bar{\rho}_E$. Hence the ratio between the two is

$$\frac{3(1+k_2')(1+k_2-h_2)\rho_W}{5k_2\left[1 - \frac{3}{5}\left(\frac{\rho_W}{\bar{\rho}_E}\right)(1+k_2'-h_2')\right]\bar{\rho}_E} = 0.22 \qquad \text{(A1)}$$

for the values $k_2 = 0.30$, $k_2' = -0.31$, $h_2 = 0.61$, and $h_2' = -1.00$ (Lambeck, 1980, pp. 13-14). Thus the ocean tide effect is 22 percent that of the solid earth tide. Hence once the effect of the solid earth tide on the node of Lageos' orbit is found, the ocean tide effect immediately follows.

PRECEDING PAGE BLANK NOT FILMED

ORIGINAL PAGE IS
OF POOR QUALITY

The solid earth tide is found next. Goad (1977) argues that for the sake of easy integration the solid earth tidal disturbing potential should be expressed in terms of the satellite's Keplerian elements (a, e, I, ω, Ω, M) referred to the earth's equator and the moon's Keplerian elements ($\hat{a}^*$, $\hat{e}^*$, $\hat{I}^*$, $\hat{\omega}^*$, $\hat{\Omega}^*$, $\hat{M}^*$) referred to the ecliptic. (See also Musen and Estes, 1972.) This will be done here. However, Goad's (1977, equation I.7) expression will not be used here since it contains some errors, as Goad himself realized; instead a slightly different derivation is sketched below.

Kaula (1964) shows how to obtain the solid earth tidal disturbing potential U^{SE} expressed in terms of the satellites's and moon's equatorial Keplerian elements from the tide-raising potential

$$U = \frac{GM_M}{r^*} \sum_{\ell=2}^{\infty} \left(\frac{r}{r^*}\right)^{\ell} \sum_{m=0}^{\ell} \sum_{i=1}^{2} \frac{(\ell-m)!}{(\ell-m)!} (2-\delta_{0m})\, Y_{\ell mi}(\theta,\lambda)\, Y_{\ell mi}(\theta^*,\lambda^*) \qquad \text{(A2)}$$

expressed in terms of the spherical harmonics $Y_{\ell m1}(\theta,\lambda) = P_{\ell m}(\cos\theta)\cos m\lambda$, $Y_{\ell m2}(\theta,\lambda) = P_{\ell m}(\cos\theta)\sin m\lambda$ which refer to the earth's equatorial system. The lunar equatorial spherical harmonics $Y_{\ell mi}(\theta^*,\lambda^*)$ may be expressed in terms of the ecliptic colatitude $\hat{\theta}^*$ and longitude $\hat{\lambda}^*$ using (Messiah, 1963, pp. 1073-1074)

$$Y_{\ell mi}(\theta^*,\lambda^*) = \sum_{s,t} A_{\ell mist}\, Y_{\ell st}(\hat{\theta}^*,\hat{\lambda}^*),$$

where the coefficients $A_{\ell mist}$ depend on the elements of the rotation matrix between the equatorial and ecliptic coordinate systems. After substituting this expression in (A2) and thereafter following Kaula's (1964) treatment gives $U^{SE} = \sum U^{SE}_{\ell mspqhj}$, where

$$U^{SE}_{\ell mspqhj} = \sum_{i=1}^{2} \sum_{t=1}^{2} \frac{GM_M}{R_E} k_\ell \frac{(2-\delta_{0m})\,(\ell-m)!}{2\quad(\ell+m)!} \left(\frac{R_E}{a}\right)^{\ell+1} \left(\frac{R_E}{\hat{a}^*}\right)^{\ell+1} F_{\ell mh}(I)\, F_{\ell sp}(\hat{I}^*)\, G_{\ell hj}(e)\, G_{\ell pq}(\hat{e}^*)\, A_{\ell mist}$$

ORIGINAL PAGE IS
OF POOR QUALITY

$$\cdot \begin{cases} -\cos\left[v_{\ell mhj} + \hat{v}^{*}_{\ell spq} - (t+i)\frac{\pi}{2}\right] + \cos\left[v_{\ell mhj} - \hat{v}^{*}_{\ell spq} + (t-i)\frac{\pi}{2}\right] & \ell-m \text{ even}, \ell-s \text{ even} \\ -\sin\left[v_{\ell mhj} + \hat{v}^{*}_{\ell spq} - (t+i)\frac{\pi}{2}\right] - \sin\left[v_{\ell mhj} - \hat{v}^{*}_{\ell spq} + (t-i)\frac{\pi}{2}\right] & \ell-m \text{ even}, \ell-s \text{ odd} \\ -\sin\left[v_{\ell mhj} + \hat{v}^{*}_{\ell spq} - (t+i)\frac{\pi}{2}\right] + \sin\left[v_{\ell mhj} - \hat{v}^{*}_{\ell spq} + (t-i)\frac{\pi}{2}\right] & \ell-m \text{ odd}, \ell-s \text{ even} \\ +\cos\left[v_{\ell mhj} + \hat{v}^{*}_{\ell spq} - (t+i)\frac{\pi}{2}\right] + \cos\left[v_{\ell mhj} - \hat{v}^{*}_{\ell spq} + (t-i)\frac{\pi}{2}\right] & \ell-m \text{ odd}, \ell-s \text{ odd} \end{cases} \tag{A3}$$

where

$$v_{\ell mhj} = (\ell-2h)\,\omega + (\ell-2h+j)\,M + m\Omega,$$

$$\hat{v}^{*}_{\ell spq} = (\ell-2p)\,\hat{\omega}^{*} + (\ell-2p+q)\,\hat{M}^{*} + s\hat{\Omega}^{*}.$$

Here k_ℓ is the solid earth Love number of degree ℓ, M_M the mass of the moon, R_E the equatorial radius of the earth, and G the universal constant of gravitation.

For the 18.6 year tide $\ell = 2$, $m = 0$, $s = 1$, $p = 1$, $q = 0$, $h = 1$, and $j = 0$, so that (A3) becomes

$$U^{SE}_{2011010} = \frac{GM_M}{R_E}\, k_2 \left(\frac{R_E}{a}\right)^3 \left(\frac{R_E}{\hat{a}^{*}}\right)^3 F_{201}(I)\, F_{211}(\hat{I}^{*})\, G_{210}(e)\, G_{210}(\hat{e}^{*})$$

$$\cdot \left\{ A_{20111} \sin\hat{\Omega}^{*} - A_{20112} \cos\hat{\Omega}^{*} \right\} \tag{A4}$$

The coefficients A_{20111} and A_{20112} can easily be found from the addition theorem for spherical harmonics (e.g., Kaula, 1964, p. 67), since $m = 0$ in the above equation. They are $A_{20111} = 0$ and $A_{20112} = \sin\epsilon\cos\epsilon$, where ϵ is the obliquity of the ecliptic. Using these values in (A4) and noting that $G_{210}(e) \cong G_{210}(\hat{e}^{*}) \cong 1$ because of the nearly circular orbits of the moon and Lageos give

$$U^{SE}_{2011010} = -\frac{GM_M}{R_E}\, k_2 \left(\frac{R_E}{a}\right)^3 \left(\frac{R_E}{\hat{a}^{*}}\right)^3 F_{201}(I)\, F_{211}(\hat{I}^{*}) \sin\epsilon\cos\epsilon\cos\Omega^{*}$$

whi· h varies sinusoidally with time with a period of 18.6 years. Substituting this expression in the Lagrange planetary equation for $d\Omega/dt$ (e.g., Kaula, 1968, p. 166) and integrating with respect to time yields

$$\Delta\Omega \cong \frac{-9\, GM_M\, k_2}{4\sqrt{GM_E a}\; R_E\; \hat{\Omega}^*} \left(\frac{R_E}{a}\right)^3 \left(\frac{R_E}{\hat{a}^*}\right)^3 \cos I \sin \hat{I}^* \cos \hat{I}^* \sin \epsilon \cos \epsilon \sin \hat{\Omega}^*$$

for the effect of the 18.6 year solid earth tide on the node of Lageos' orbit. Multiplying this by $\cap$ 22 as dictated by (A1) and using the numerical values $\epsilon = 23.44$ degrees, $\hat{I}^* = 5.15$ degrees, etc. (e.g., Kaula, 1968, p. 186) yields the effect of the 18.6 year global equilibrium ocean tide as given by (1).

REFERENCES

Agnew, D. C., and W. E. Farrell, Self-consistent equilibrium ocean tides, *Geophys. J. R. Astron. Soc.*, *55*, 171-181, 1978.

Andrews, J. T., and R. G. Berry, Glacial inception and disintegration during the last glaciation, in *Annual Review of Earth and Planetary Sciences*, vol. 6, edited by F. A. Donath, pp. 205-228, Annual Reviews, Inc., Palo Alto, 1978.

Cathles, L. M., *The Viscosity of the Earth's Mantle*, Princeton University Press, Princeton, 1975.

Currie, R. G., The spectrum of sea level from 4 to 40 years, *Geophys. J. R. Astron. Soc.*, *46*, 513-520, 1976.

Darwin, G. H., On the bodily tides of viscous and semi-elastic spheroids, and on the ocean tides upon a yielding nucleus, *Phil. Trans. Roy. Soc. London*, part 1, *170*, 1-35, 1879. (Reproduced in *Scientific Papers* by G. H. Darwin, vol. 2, pp. 1-32, Cambridge University Press, London, 1908.)

Gilbert, F., and A. M. Dziewonski, An application of normal mode theory to the retrieval of structural parameters and source mechanisms from seismic spectra, *Phil. Trans. Roy. Soc. London*, *A278*, 187-269, 1975.

Goad, C. C., Application of Digital Filtering to Satellite Geodesy, *NOAA Tech. Rep.* NOS 71 NGS 6, National Oceanic and Atmospheric Administration, Washington, D. C., May 1977.

Goldreich, P., and A. Toomre, Some remarks on polar wandering, *J. Geophys. Res.*, *74*, 2555-2567, 1969.

Hays, J. D., J. Imbrie, and N. J. Shackleton, Variations in the earth's orbit: pacemaker of the ice ages, *Science*, *194*, 1121-1132, 1976.

Hendershott, M. C., The effects of solid earth deformation on global ocean tides, *Geophys. J. R. Astron. Soc.*, *29*, 389-402, 1972.

Kaula, W. M., Tidal dissipation by solid friction and the resulting orbital evolution, *Rev. Geophys.*, *2*, 661-685, 1964.

Kaula, W. M., Geophysical implications of satellite determinations of the earth's gravitational field, *Space Sci. Rev.*, *7*, 769-794, 1967.

Kaula, W. M., *An Introduction to Planetary Physics*, John Wiley, New York, 1968.

Kozai, Y., Long-range analysis of satellite observations, in *Trajectories of Artificial Celestial Bodies as Determined From Observations, COSPAR-IAU-IUTAM Symposium*, edited by J. Kovalevsky, pp. 44-52, Springer-Verlag, New York, 1966.

Lambeck, K., *The Earth's Variable Rotation*, Cambridge University Press, London, 1980.

Lerch, F. J., B. H. Putney, C. A. Wagner, and S. M. Klosko, Goddard Earth Models for oceanographic applications (GEM 10B and 10C), *Marine Geodesy*, *5*, 145-187, 1981.

Lowman, P. D., A global tectonic activity map, *Bull. Int. Assoc. Eng. Geology*, *23*, 37-49, 1981.

Lowman, P. D., A more realistic view of global tectonism, *J. Geol. Ed.*, *30*, 97-107, 1982.

Lyttleton, R. A., *The Stability of Rotating Liquid Masses*, Cambridge University Press, London, 1953.

Markowitz, W., Independent polar motions, optical and Doppler; Chandler uncertainties, Report to IAU Commissions 19 and 31, Montreal, August, 1979.

McAdoo, D. C., On the compensation of geoid anomalies due to subducting slabs, *J. Geophys. Res.*, *87*, 8684-8692, 1982.

McKenzie, D. P., The viscosity of the lower mantle, *J. Geophys. Res.*, *71*, 3995-4010, 1966.

Messiah, A., *Quantum Mechanics*, vol. 2, North-Holland, Amsterdam, 1963.

Musen, P., and R. Estes, On the tidal effects in the motion of artificial satellites, *Celest. Mech.*, *6*, 4-21, 1972.

Nakiboglu, S. M., Hydrostatic figure and related properties of the earth, *Geophys. J. R. Astron. Soc.*, *57*, 639-648, 1979.

Nakiboglu, S. M., and K. Lambeck, Deglaciation effects on the rotation of the earth, *Geophys. J. R. Astron. Soc.*, *62*, 49-58, 1980.

Nakiboglu, S. M., and K. Lambeck, Corrigendum, *Geophys. J. R. Astron. Soc.*, *64*, 559, 1981.

O'Connell, R. J., Pleistocene glaciation and the viscosity of the lower mantle, *Geophys. J. R. Astron. Soc.*, *23*, 299-327, 1971.

O'Keefe, J. A., D. P. Rubincam, D. E. Smith, and C. A. Wagner, Relaxation time of non-hydrostatic J_2 and the viscosity of the deep mantle, (Abstract), *Eos*, *60*, 317, 1979.

Paddack, S. J., On the angular momentum of the solid earth, *J. Geophys. Res.*, *72*, 5760-5762, 1967.

Peltier, W. R., Mantle convention and viscosity, in *Physics of the Earth's Interior*, edited by A. M. Dziewonski and E. Boschi, pp. 362-431, North-Holland, New York, 1980.

Peltier, W. R., Ice age geodynamics, in *Annual Review of Earth and Planetary Sciences*, vol. 9, edited by G. W. Wetherill, pp. 199-225, Annual Reviews Inc., Palo Alto, 1981.

Peltier, W. R., and P. Wu, Mantle phase transitions and the free air gravity anomalies over Fenno-scandia and Laurentia, *Geophys. Res. Lett.*, *9*, 731-734, 1982.

Peltier, W. R., and P. Wu, Deglaciation induced polar motion and variations of lod, paper presented at the Fifth Annual Geodynamics Program Conference and Crustal Dynamics Project Review, Washington, D. C., January 24-28, 1983.

Peltier, W. R., W. E. Farrell, and J. A. Clark, Glacial isostasy and relative sea level: a global finite element model, *Tectonophysics*, *50*, 81-110, 1978.

Proudman, J., The condition that a long-period tide shall follow the equilibrium law, *Geophys. J. R. Astron. Soc.*, *3*, 244-249, 1960.

Rapp, R. H., The earth's gravity field, *Geophys. Surveys*, *2*, 193-216, 1975.

Rossiter, J. R., An analysis of annual sea level in European waters, *Geophys. J. R. Astron. Soc.*, *13*, 259-299, 1962.

Rubincam, D. P., Gravitational potential energy of the earth: a spherical harmonic approach, *J. Geophys. Res.*, *84*, 6219-6225, 1979.

Rubincam, D. P., On the secular decrease in the semimajor axis of Lageos's orbit, *Celest. Mech.*, *26*, 361-382, 1982.

Sabadini, R., and W. R. Peltier, Pleistocene deglaciation and the earth's rotation: implications for mantle viscosity, *Geophys. J. R. Astron. Soc.*, *66*, 553-578, 1981.

Sabadini, R., D. A. Yuen, and E. Boschi, Interaction of cryospheric forcings with rotational dynamics has consequences for ice ages, *Nature*, *296*, 338-341, 1982a.

Sabadini, R., D. A. Yuen, and E. Boschi, Polar wandering and the forced responses of a rotating, multilayered, viscoelastic planet, *J. Geophys. Res.*, *87*, 2885-2903, 1982b.

Sanchez, B. V., The enhanced nodal equilibrium ocean tide and polar motion, *NASA/GSFC Tech. Memo.* 80592, November, 1979.

Smith, D. E., and P. J. Dunn, Long term evolution of the Lageos orbit, *Geophys. Res. Lett.*, *7*, 437-440, 1980.

Stacey, F. D., *Physics of the Earth*, 2nd ed., John Wiley, New York, 1977.

Wang, C.-Y., Earth's zonal deformations, *J. Geophys. Res.*, *71*, 1713-1720, 1966.

Weertman, J., Creep laws for the mantle of the earth, *Phil. Trans. R. Soc. London*, *A288*, 9-26, 1978.

Wu, P., and W. R. Peltier, Viscous gravitational relaxation, *Geophys. J. R. Astron. Soc.*, *70*, 435-485, 1982.

Yoder, C. F., J. G. Williams, J. O. Dickey, B. E. Schutz, R. J. Eanes, and B. D. Tapley, $\dot{J}_2$ from Lageos, paper presented at the Fifth Annual Geodynamics Program Conference and Crustal Dynamics Program Review, Washington, D. C., January 24-28, 1983.

Yuen, D. A., R. Sabadini, and E. V. Boschi, Viscosity of the lower mantle as inferred from rotational data, *J. Geophys. Res.*, *87*, 10745-10762, 1982.

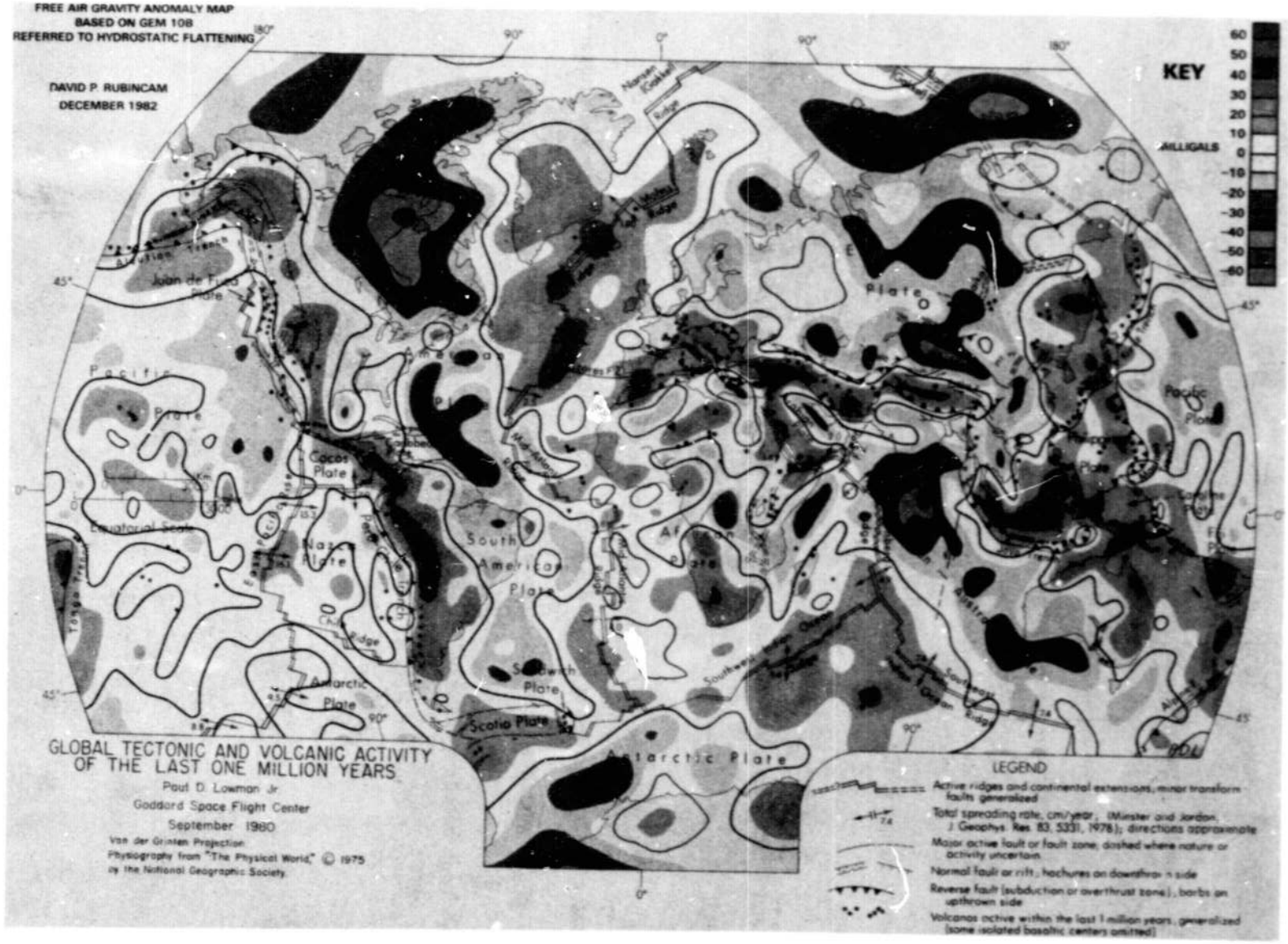

Plate 1. The GEM 10B free air gravity anomalies referred to the earth's hydrostatic figure. Van der Grinten projection.

ORIGINAL PAGE IS
OF POOR QUALITY

ORIGINAL PAGE IS
OF POOR QUALITY

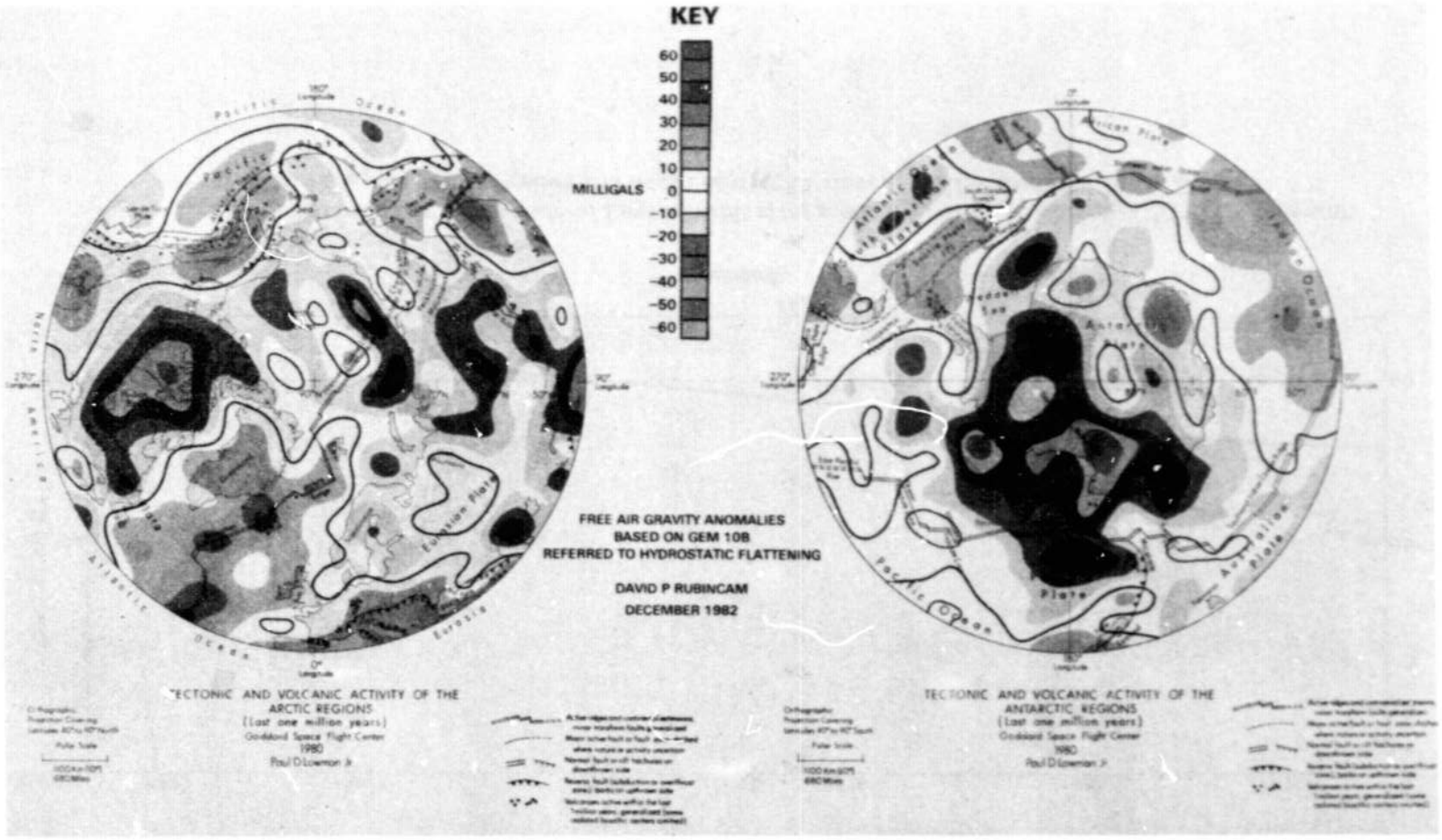

Plate 2. The GEM 10B free air gravity anomalies referred to the earth's hydrostatic figure. Polar orthographic projection.

ORIGINAL PAGE IS
OF POOR QUALITY

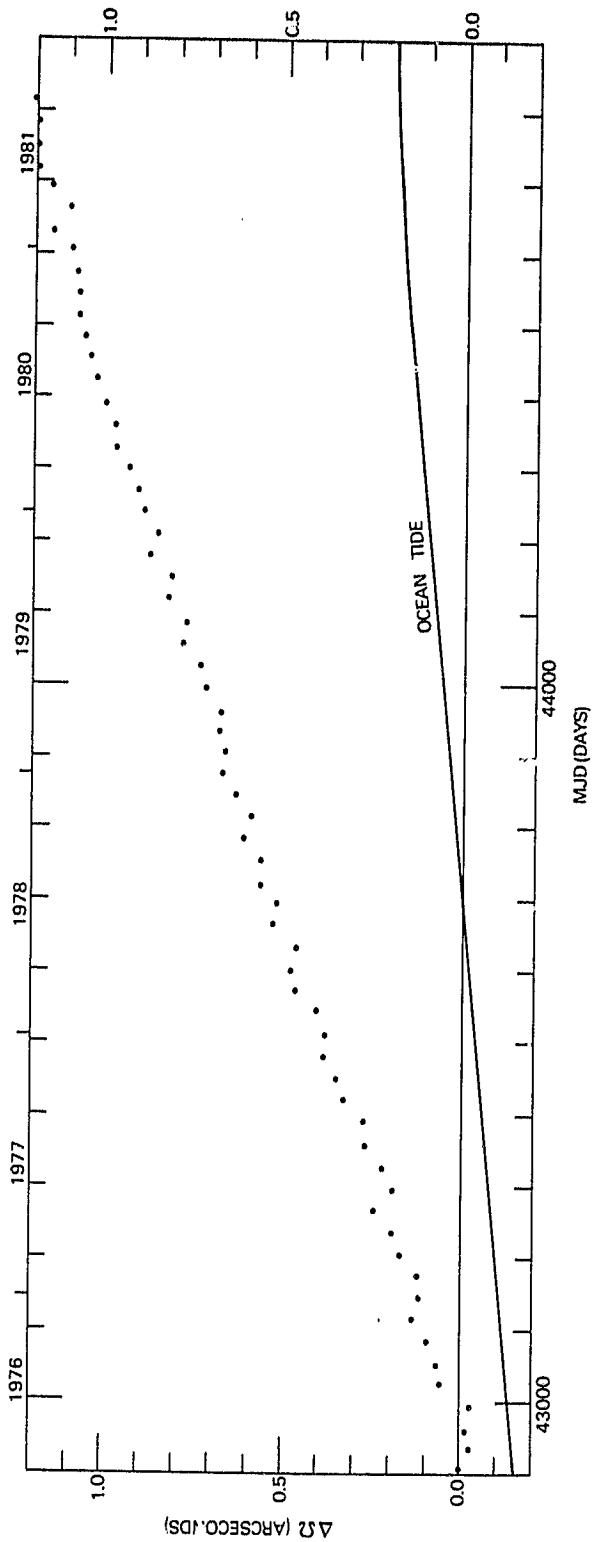

Figure 1. Plot of the residuals in the node of Lageos' orbit after modeling the orbit with the GEODYN program; also the 18.6 year global equilibrium ocean tide (solid curve). MJD = Modified Julian Date.

ORIGINAL PAGE IS
OF POOR QUALITY

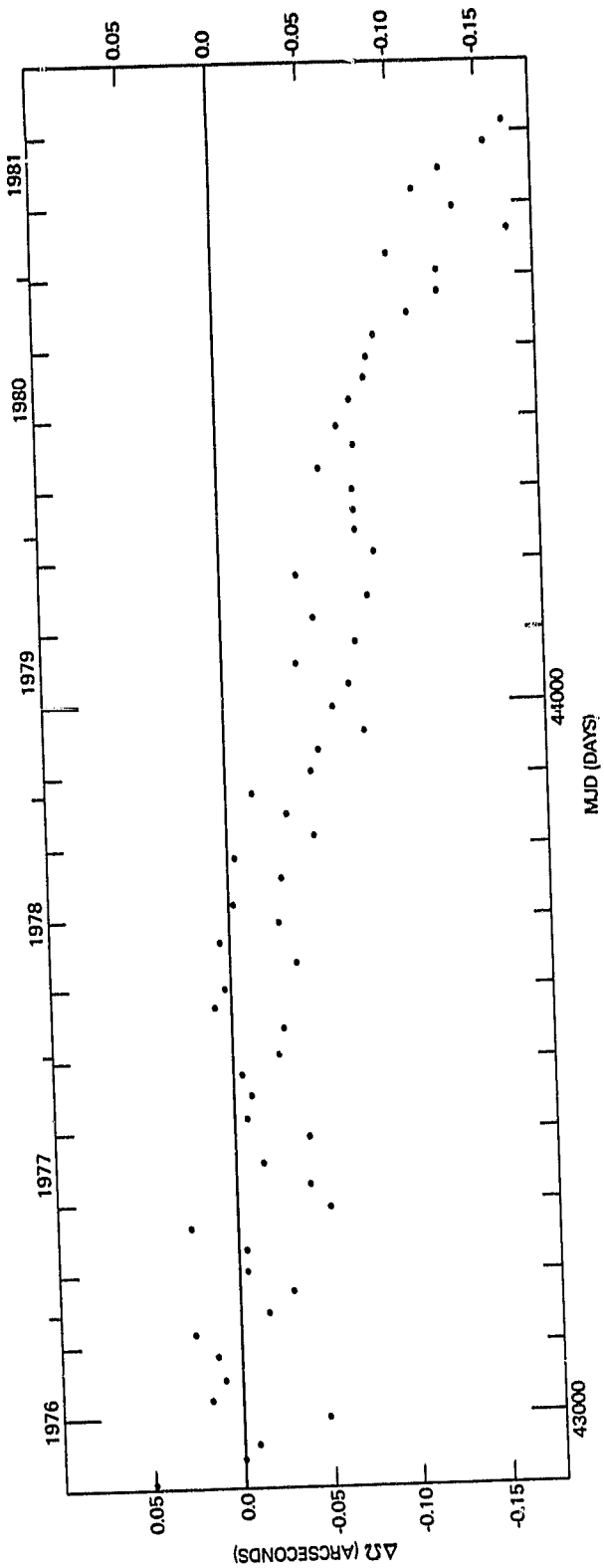

Figure 2. Plot of the residuals in the node after removing the 18.6 year ocean tide perturbation, the constant, and the slope, leaving only the curvature presumably due to postglacial rebound.

ORIGINAL PAGE IS
OF POOR QUALITY

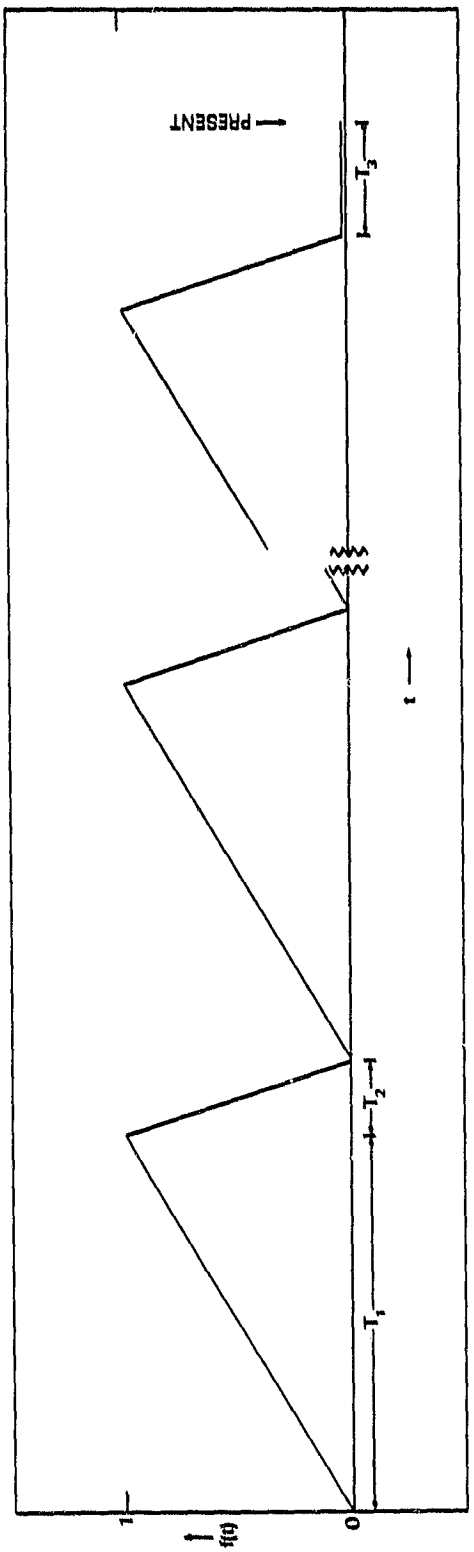

Figure 3. Assumed ice sheet history for Laurentide Canada. T_1 is the characteristic accretion time and T_2 is the characteristic disintegration time, while T_3 is the elapsed time from the end of disintegration to the present.

FIGURE CAPTIONS

Plate 1. The GEM 10B free air gravity anomalies referred to the earth's hydrostatic figure. Van der Grinten projection.

Plate 2. The GEM 10B free air gravity anomalies referred to the earth's hydrostatic figure. Polar orthographic projection.

Figure 1. Plot of the residuals in the node of Lageos' orbit after modeling the orbit with the GEODYN program; also the 18.6 year global equilibrium ocean tide (solid curve). MJD = Modified Julian Date.

Figure 2. Plot of the residuals in the node after removing the 18.6 year ocean tide perturbation, the constant, and the slope, leaving only the curvature presumably due to postglacial rebound.

Figure 3. Assumed ice sheet history for Laurentide Canada. T_1 is the characteristic accretion time and T_2 is the characteristic disintegration time, while T_3 is the elapsed time from the end of disintegration to the present.

Table 1

Preferred Values for the Laurentide Ice Sheet Parameters

Parameter	Symbol	Value
Radius of Ice Sheet	α	15 Degrees
Colatitude of Center of Ice Sheet	β	25 Degrees
Maximum Mass of Ice Sheet	M_o	1.8×10^{19} kg
Characteristic Accretion Time	T_1	112 000 Years
Characteristic Disintegration Time	T_2	13 000 Years
Elapsed Time Since the End of Disintegration to the Present	T_3	5000 Years

Table 2

Values for $\kappa_j^2 = 1/r_j^2$ and $\tau_j^2 = 1/s_j^2$ for Models L1 and L2

Model	Mode	κ_j^2 (yr)	τ_j^2 (yr)
L1	CO	−3592	2670
	MO	−4737	3890
L2	CO	−72 808	40 984
	LO	−103 171	13 123

Derived from Tables 8 and 9 of Wu and Peltier (1982). Only those values which contribute significantly to $\dot{J}_2$ are shown here.

TABLE CAPTIONS

Table 1. Preferred values for the Laurentide ice sheet parameters.

Table 2. Values for $\kappa_j^2 = 1/r_j^2$ and $\tau_j^2 = 1/s_j^2$ for models L1 and L2. Derived from Tables 8 and 9 of Wu and Peltier (1982). Only those values which contribute significantly to $\dot{J}_2$ are shown here.